The Assessment of Sediment Transport Rates by Automated Digital Photogrammetry

M. Stojic, J. Chandler, P. Ashmore, and J. Luce

Abstract

Automated DEM acquisition methods are used to generate dense elevation models of a controlled experimental flume used to simulate sediment transport in a braided stream. A Pentax 645 non-metric camera was used to acquire all imagery, and uncertainities concerning the interior orientation of the camera were overcome using a self-calibrating bundle adjustment. The ERDAS IMAGINE OrthoMAX software package was used to derive all DEMs, and derived elevation models were used in a variety of ways to provide data of geomorphological significance. A study of the quality of derived data suggests that reliable estimates of sediment transport can theoretically be derived from the detection of morphological change alone, but it is very difficult to achieve in practice.

Introduction

Geomorphology is concerned with the description and measurement of landforms and landform change. Testing of geomorphological theory and modeling of processes increasingly requires high resolution quantitative data of topography and topographic change at a wide range of scales. Photogrammetry has been used as a source of landform information in a variety of geomorphic applications (Welch and Jordan, 1983; Collin and Chisholm, 1991) but the advent of analytical and, more recently, digital photogrammetry has opened new applications for photogrammetry in the acquisition of geomorphic data (Lane *et al.*, 1993; Fryer *et al.*, 1994; Brunsden and Chandler, 1996; Dixon *et al.*, 1996). The principal advantage of photogrammetry over ground survey is the potential to acquire high spatial resolution, continuous data from photographs which provide a permanent record of landform. This becomes even more advantageous in situations in which detailed survey of rapidly changing forms is required.

Previous applications of analytical photogrammetry to landform change include studies of slope morphology and stability. Oblique aerial photographs have been used to monitor slope instability at discrete points (Fraser, 1983) and to obtain topographic data for describing slope morphology (Chandler *et al.*, 1987; Chandler and Moore, 1989) and for quantifying change over time (Chandler and Brunsden, 1995).

Fluvial geomorphology applications have largely been restricted to mapping of planimetric changes from sequential aerial photography over years or decades (Lewin and Weir, 1977; Collins and Moon, 1979). Application of photogrammetry is limited by the need to survey topography beneath the water surface. However, Lane *et al.* (1993; 1994) utilized a combination of analytical photogrammetry and ground survey to measure changes in river bed topography. Grid comparison techniques were employed for multi-temporal surface comparison to quantify and visualize spatial patterns of change. Inter-epoch comparisons were combined with information on upstream sediment supply to assess a particular reach and its contribution to the total bedload transport rate. Distributed patterns of the time-averaged bedload transport rate were also assessed.

In hydraulic models of river channel processes, the problem of surveying beneath the water can be circumvented by draining the model when photography is required. In the past, conventional (analog) photogrammetry has been used for this purpose (Jäggi, 1975), but the potential of deriving very dense DEMs using the fully automated methods associated with digital photogrammetry has not been investigated. In this paper, we describe the application of close-range automated digital photogrammetry to the measurement of bed topography and topographic change in small-scale laboratory river models. One particular aim was to investigate the possibility of quantifying the sediment budget and, hence, sediment transport rates solely by determining volumetric change. An exhaustive assessment of the accuracy of derived topographic surfaces suggests that this is possible provided that all components of the digital measurement system are carefully calibrated and controlled.

The Physical River Model and Data Acquisition

The river model in which all experimental work was performed was an approximately 1:20 generic scale hydraulic model of a gravel-bed, braided stream (Figure 1). The model was developed in a laboratory flume 2.9 m wide by 11.5 m long. The sediment was a widely graded, medium-coarse sand with median grain diameter of 0.7 mm, and maximum diameter of 4 mm. Flume slope was 0.012 and water discharge was 1.5 l s^{-1}. River morphology was created by beginning with a straight channel with trapezoidal cross-section and allowing the natural channel morphology to develop over the course of a few hours. Morphological development was initiated first by establishing a sinuous channel and eventually, after two hours, a braided channel which evolved and widened over the course of the experiment.

River Model Conditions

Sediment input at the upstream end of the flume was supplied by a calibrated sediment feed device, and the output at

M. Stojic, P. Ashmore, and J. Luce are with the Department of Geography, University of Western Ontario, London, Ontario N6A 5C2, Canada.

J. Chandler is with the Department of Civil Engineering, Loughborough University, Loughborough, LE11 3TU, England.

M. Stojic is currently with ERDAS Inc., 2801 Buford Highway NE, Suite 300, Atlanta, GA 30329-2137.

J. Luce is currently with Aquafor Beech, 14 Abacus Road, Brampton, Ontario L6T 5B7, Canada.

Photogrammetric Engineering & Remote Sensing, Vol. 64, No. 5, May 1998, pp. 387–395.

0099-1112/98/6405–387$3.00/0

the downstream end was accumulated in a large drum. Flow was recirculated, but sediment was not. The flow was stopped at regular intervals of 5, 10, or 15 minutes to allow photographs to be taken of the whole river bed once the water had drained and for removal and weighing of the sediment accumulated in the output drum. The volume of sediment input was calculated by knowing the feed rate and by timing the period for which the feeder was turned on. The direct measurement of sediment input and output is a unique and crucial part of the experiment which allows all the components of the sediment mass budget to be completely quantified without resort to unmeasured residual terms. This mass balance serves as an independent check on the accuracy of the photogrammetric survey because the net change in sediment storage in the flume at each time step is the difference between sediment input and output volume.

Photogrammetric Data Acquisition

Detecting change through the use of multi-temporal photogrammetric surveys requires careful consideration and definition of a datum. Any detected change must be attributable to sediment transport processes and not to minor datum shifts. To ensure a stable datum for the duration of the experimental work, a dense array of photo-control targets was established. Thirty-four square targets (approximately 30 mm by 30 mm) were placed on top of bolts and secured to the base of the flume. The targets were distributed in three rows, each being separated by a distance of approximately 1.0 to 1.5 metres (Figures 1 and 2). The preliminary stages of photogrammetric data acquisition involved the collection of survey data necessary to establish the coordinates of control points to a high precision. Coordinates were determined by a three-dimensional intersection technique using measurements acquired from three survey stations. A Sokkia SET4B Total Station was used, which had an angular resolution of 5 seconds. The survey stations were approximately 4 metres above the ground and approximately 6 to 7 metres perpendicular to the flume. Each control point target was measured independently three times from all three survey stations, thus providing replicate data. The GAP software package developed at City University, London, UK, was employed which used the "three-dimensional variation of coordinates" technique to provide the best estimates for the target positions (Cooper, 1987). The root-mean-square precision for the *XYZ* coordinates was calculated to be 0.19 mm, 0.41 mm, and 0.19 mm, respectively.

No metric camera was available at the time of the flume experiments. Consequently, a Pentax 645 medium format non-metric camera was used. The approximate focal length was 55 mm, with a photographic format size of 55 mm by 41 mm. The focusing range was pre-set to 4 metres at *f*8. Kodak TMAX 120, 400 ASA, black-and-white photography was used. This camera lacks fiducial marks, and the only reference points suitable for defining a reference system in the image space were the corners of camera format (Smith, 1987).

The camera was supported on a gantry crane approximately 4 metres above the sediment surface. Illumination was provided by four floodlights attached to the crane and positioned in pairs approximately 1 metre from each side of the camera. Vertical photographs were obtained in 39 separate epochs. The elapsed time between photography ranged from 5 to 35 minutes, but in most cases was either 10 or 15 minutes. The water flow and sediment feed were stopped, and the flume was allowed to drain, for each set of photographs. Eight photographs comprising a strip were taken to obtain full stereoscopic coverage of the flume. Using a photographic base of 1.5 m, adjacent photographs provide for 60 percent overlap and a photo scale of 1:70. At least six control points lay in the overlapping areas of any two photographs of a stereoscopic pair taken from the strip.

Figure 1. Oblique photograph of the experimental flume with small-scale river model.

Convergent and oblique photographs were obtained from both ends of the flume prior and subsequent to the first and last epochs. The geometric configuration comprised four photographs taken from the upstream end of the flume and two photographs taken from the downstream end of the flume (Figure 3). Two of the cameras from the upstream end of the flume were intentionally rotated 90 degrees about the optical axis of the camera. Studies indicate that the use of highly convergent oblique photography as part of a photogrammetric net contributes to greater precision in the recovery of elements of interior and exterior orientation (Kenefick *et al.*, 1972; Granshaw, 1980; Chandler *et al.*, 1989). Another advantage of such a configuration is a reduction in correlation between interior and exterior orientation parameters.

Photogrammetric Data Processing

Image Scanning

In order to use digital photogrammetry to generate DEMs of the sand surface, hardcopy negatives were converted to soft-

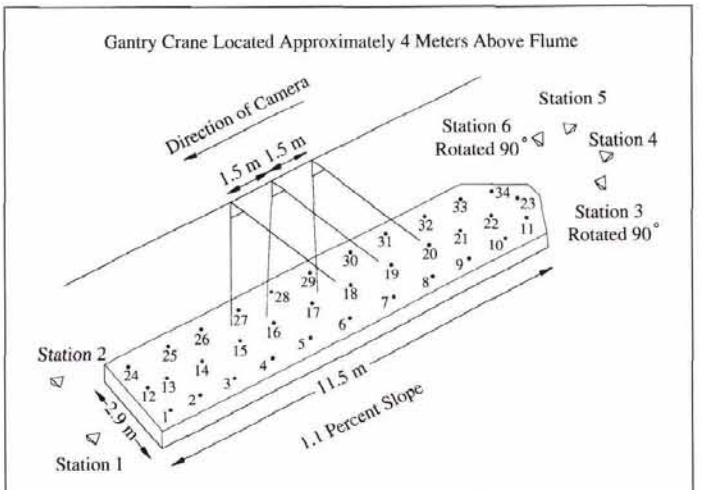

Figure 2. Conceptual view of flume showing camera station configuration and control survey. Numbered points on the river model are control-point positions.

Figure 3. Example stereo-pair of close-range vertical photographs.

copy data. To resolve constraints of data processing time and storage, an appropriate scanning resolution was determined by balancing the coverage of a pixel on the ground with computer storage space. According to Nolette *et al.* (1992), the attainable precision of object-space coordinates on the model is a function of scanning resolution. Using a Helava DSW100 Digital Scanning Workstation at City University, the negatives were scanned at a resolution of 12.5 μm utilizing 256 levels of grey. At the scale of the photography, each pixel represents an area of 0.84 by 0.84 mm on the flume bed. Such ground coverage is adequate in representing particles equal to and greater than 1 mm in diameter.

Self-Calibrating Bundle Adjustment

Current commercial softcopy photogrammetry software packages do not have the capability to estimate the interior-orientation parameters of a camera, and this was essential for res tituting the non-metric imagery. Interior-orientation parameters were derived using the self-calibrating bundle adjustment (SCBA) program GAP developed at City University. This implements the modified and extended collinearity equations to model the inner cone of the camera (Kenefick *et al.*, 1972; Albertz and Kreiling, 1989). The collinearity condition provides the numerical framework necessary to define the SCBA, and, when augmented by equations to model the camera's interior orientation, the functional model can be defined. The GAP program was modified to incorporate an additional affine transformation parameter which compensates for the rotation of the x and y image coordinate system (Patias and Streilein, 1996).

Row and column pixel coordinates for each format corner and control points were measured manually using the ERDAS IMAGINE 8.2 software package. The position of each corner of format was established by intersecting the horizontal and vertical edges of the image format corners. This approach provided a consistent technique for locating the format corners on each image. Control point pixel coordinates were transformed to the photo-coordinate system using a two-dimensional affine transformation.

The stochastic properties of the control-point coordinates and photo coordinates were incorporated into the SCBA. Standard errors of 5 and 6 μm were assigned to the stochastic model for photo coordinates in the x and y directions, respectively. The datum for self calibration was defined through four widely separated control points constrained by the standard errors estimated during the control survey adjustment.

The lack of calibration data for the format corners and consequent use of arbitrarily assigned values meant that it could not be assumed that photo-coordinate scale was invariant in the x and y photo-coordinate directions. Tests were undertaken to determine the effect of the differential scale within the SCBA. A differential scale factor was derived by internally estimating focal length changes in the x and y directions, and this was used to correct the initial y photo coordinates assigned and used for establishing the affine parameters during interior orientation. Re-processing the SCBA and re-estimating this differential scale parameter confirmed that the revised format corner coordinates had been corrected.

Five interior-orientation parameters were finally derived along with estimates of their standard errors (Table 1).

The K_3 coefficient for radial lens distortion and the P_1 and P_2 coefficients for tangential lens distortion were removed from the estimation process because the standard errors were greater than the parameters. The average root-mean-square error for photo-coordinate residuals in the x and y directions for each of the six photographs was approximately 5.0 μm for both directions. The accuracy of the photo-coordinate measurements is approximately 5 μm.

The estimated interior- and exterior-orientation parameters were then used to re-compute control-point coordinates, and the differences between these and the original surveyed control-point coordinates were determined to provide an additional check on the accuracy of the photogrammetric bundle. Mean differences were 0.0025, 0.0007, and 0.0014 metres for the X, Y, and Z coordinates, respectively. Larger X-coordinate residual errors could be attributed to the optical axis for the oblique photography being directed parallel to the X ordinate. The resulting effect contributes to a lower precision in the estimation of interior-orientation parameters because imaged points remain distributed over the central portion of a photograph. The result of this is a weak geometry within the photograph obtained from Camera Station One at the downstream end of the flume. The redundancy of four photographs at the upstream end of the flume, coupled with the introduction of photography obtained from cameras oriented 90 degrees from the optical axis, resulted in lower residuals in the X, Y, and Z coordinates for control points lying at the upstream end of the flume (i.e., points 11, 22, 33, and 34). The precision for control-point coordinates

TABLE 1. ESTIMATED INTERIOR-ORIENTATION PARAMETERS AND STANDARD ERRORS FROM THE SELF-CALIBRATING BUNDLE ADJUSTMENT

	Interior Orientation Parameters	Standard Error
Focal Length (mm)	58.9237	0.0406
x_p (mm)	0.1808	0.0455
y_p (mm)	−0.2076	0.0932
K_1 (m^{-2})	−21.604	1.211
K_2 (m^{-4})	3958.2	1616.5

in the X direction was lower because the camera axis was oriented in the general direction of the X axis of the ground-coordinate system.

The *a posteriori* variance factor derived from photo-coordinate residuals and control-point residuals, and the standard errors associated with these measurements, were used as a global comparative measure of accuracy. The estimated *a posteriori* variance factor of 1.523 is slightly greater than unity, thus indicating the presence of either uncompensated systematic errors or a minor scaling error in the stochastic model. Several tests were undertaken in an attempt to lower the *a posteriori* variance factor by reducing the stochastic properties associated with the x and y photo coordinates. This resulted in larger values for control-point standard errors. The optimum *a posteriori* variance factor was obtained by balancing the stochastic properties of the photo coordinates with the control-point standard errors. Minor systematic errors remain which are attributed to film deformation, uncompensated residual lens distortions, or small distortions created by the adopted method of interior orientation.

Photogrammetric Restitution within ERDAS OrthoMAX

The ERDAS IMAGINE OrthoMAX software package (ERDAS, 1995) was used to restitute the imagery and automatically extract the three-dimensional terrain models. Photogrammetric processing used a Sun Ultra SPARC 140E equipped with 4 Gb hard disk, 64 Mb of RAM, 143 MHz processing speed, and a TurboGX graphics monitor.

There are two phases of photogrammetric processing for each strip of eight photographs contained in an epoch: photogrammetric triangulation and automated DEM processing. Photogrammetric triangulation used a least-squares block bundle adjustment to estimate the exterior orientation parameters of the camera at each exposure station. The resulting exterior- and enforced interior-orientation parameters were then used for automated extraction of elevation values during the DEM processing phase.

Photogrammetric Triangulation

The eight photographs comprising each strip at each epoch were measured with a standard deviation of ± 0.15 pixel (± 1.9 µm) assigned to represent the stochastic properties of all measured photo coordinates. Interior-orientation parameters (f, x_p, y_p, and radial lens displacement at varying radial distances) determined from the SCBA and the x and y image measurements for the four corners of the format were input to establish the internal geometry of the camera. Control-point coordinates were input to establish the reference datum, and their respective standard errors were included to be used as weighted constraints in the stochastic model. Photo coordinates for each control point were measured on each image, and three additional tie points were measured on overlapping areas of each photograph. The triangulation was executed for each epoch, and solutions were derived when corrections were less than 0.0001 metres.

The accuracy of each solution was assessed by examining control- and photo-coordinate residuals. The mean root-mean-square errors for the X, Y, and Z coordinates at all epochs was 0.0018 metres, 0.0019 metres, and 0.0017 metres, respectively. Photo-coordinate residuals at all epochs indicate accuracies on the order of 1.5 and 2.2 µm in the x and y directions, respectively (Figure 6). A consistent trend illustrated higher photo-coordinate residuals in the y direction, which is typical for many bundle adjustments involving manual measurement.

A statistical test was used to assess the overall accuracy of each solution by utilizing the quadratic form of the least-squares corrections (Cooper, 1987). Using the chi-square test, the variance factor for each epoch was tested by substituting the *a posteriori* variance factor and chi-square statistic into the test. The statistical tests showed that the *a posteriori* variance factor is smaller than the *a priori* variance factor at the 95 percent confidence interval for each epoch, indicating acceptable solutions at all epochs. Results suggest that, within the constraints of the chosen stochastic model (photo coordinates ± 1.9 µm; photo control $XY \pm 2$ mm, $Z \pm 2$ mm), the selected functional model has indeed modeled the relationship between object and image and that accurate results (± 1.5 mm) would be expected.

The standard deviations of the estimated exposure-station coordinates were assessed to determine the strength of the photogrammetric net using vertical photography. Average standard deviations in the X, Y, and Z exposure-station coordinates were estimated to approximately 0.0015, 0.0015, and 0.0010 metres precision, respectively. The positional elements in the Y and Z direction for the exposure stations were assessed to determine the precision in estimating the coordinates. Assuming the camera was mounted on a uniform Y and Z plane during exposure, similar results should be achieved for each frame position and epoch. Standard deviations for the Y and Z exposure-station coordinates were computed as being higher for exposure stations located on the upstream and downstream ends of the flume and lower for exposure stations located in the central portions of the flume. The photogrammetric net comprising the central portions of the flume consisted of three overlapping photographs in the photogrammetric triangulation; the consequent increase in the redundancy of control-point measurement increased precision correspondingly.

Automatic DEM Processing

The DEM tool within OrthoMAX was used to automatically extract a DEM from image stereo-pairs. Together with the known and estimated relative and absolute orientation parameters derived from the triangulation process, a hierarchical approach to digital correlation was employed. Reduced resolution data sets (RRDS) were used to minimize the probabilities of inaccurate elevation estimation (ERDAS, 1995).

Independent DEMs were derived from the user-selected overlapping area of two images at a resolution of 7.5 mm. The selection of the 7.5-mm resolution was arbitrary, but was influenced by file handling, storage, and management issues. Another important factor influencing the final selected resolution was the time necessary to generate the individual DEMs. Derived DEMs contained approximately 110,000 points and took approximately 20 minutes to generate. Automatic DEM collection statistics were derived for each DEM extracted. The precisions derived by OrthoMAX indicate the percentage of collected points lying within categories defined by a user-specified threshold. The minimum acceptable estimated precision (i.e., 0.5 pixel) was controlled by the minimum acceptable correlation coefficient threshold (i.e., 0.6) during digital correlation (ERDAS, 1995). Four categories, were used to classify the precision with which points were collected. The categorical distribution of precision as a percentage included 22, 50, 12, and 16 percent for Good (i.e., 0 to 0.17 pixel), Fair (i.e., 0.18 to 0.33 pixel), Poor (i.e., 0.34 to 0.5 pixel), and Interpolated (greater than 0.5 pixel) categories, respectively.

Eight photographs were required to provide the necessary stereo ground coverage, requiring seven individual DEMs to be generated at each epoch. The generated DEMs were stored and displayed in the form of a raster image DEM and full coverage DEMs for each epoch were compiled from the seven independent DEMs (Figure 4). Derived elevation values for the control points shown on the full coverage DEMs were edited using a nearest-neighbor interpolation algorithm by

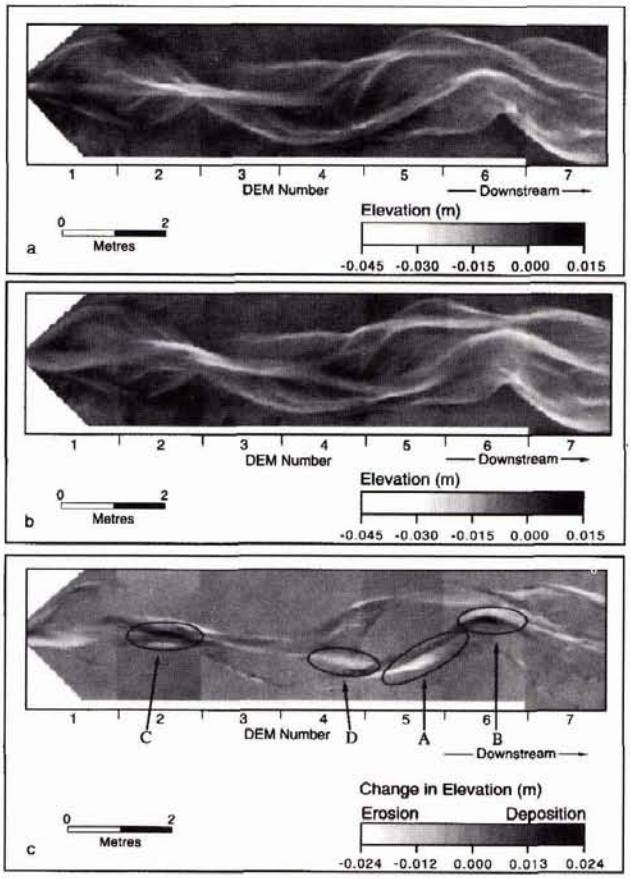

Figure 4. (a) DEM of the entire river model at time 320 minutes. (b) DEM of the entire river model at time 350 minutes. (c) DEM of difference between 320 and 350 minutes illustrating patterns and values of deposition at the downstream end of bars (B, C), erosion along a newly developing channel (D), and downstream linkage between erosion (A), and deposition (B) sites.

selecting approximately 40 source points around each control point.

Geomorphic Applications

Surveys of river channel topography and change are usually based on the interpolation of terrain between river cross-sections. Using digital photogrammetry, the complete topographic surface can be measured at high spatial and temporal resolution, without resorting to spatial interpolation or surface triangulation. There are a wide variety of applications of these DEMs, but the main objective in this case is the qualitative and quantitative analysis of morphology, morphological change, and inferred patterns of sediment transport rate in braided rivers. The experiment was devised as an explicit test, under controlled conditions, of the reliability of estimates of bed material transport calculated from net topographic change over time.

Terrain Measurement and Characterization

Accurate description and measurement of terrain allows quantitative comparison of morphology, both spatially and temporally, within a given river reach and between rivers of differing morphology. As explanations of river morphology and sedimentology make increasing use of numerical modelling techniques (Murray and Paola, 1994), there is a need for accurate data on real rivers, or of scale models, which can be used as "targets" for model verification. This comparison between the properties of model results and real stream channels has been made recently (Murray and Paola, 1996) for planimetric properties of braided channel pattern, but DEM data provide an opportunity to do this for topographic data also. Model validation would then allow model predictions to be used with greater confidence.

Channel Change and the Sediment Transfer Process

The patterns and quantities of topographic change (erosion and deposition) can be assessed by differencing of pairs of DEMs acquired at different times. Figure 4 shows DEMs for two time periods thirty minutes apart (320 and 350 minutes from the beginning of the experiment), along with a DEM of difference. The DEMs are corrected to a sloping datum parallel to the flume slope in order to reveal the morphological detail in the stream. The stream has a braided pattern in which water flows in two or more channels, separated by exposed bars of deposited sediment. Bed scour is readily apparent at the outside bank of bends and at the confluence of two or more channels.

The DEM of difference reveals some characteristic patterns of erosion and deposition. Much of the erosion and deposition is related to lateral erosion of stream banks and bars, with lateral infilling by the progradation of bar fronts into scour pools (e.g., Areas B and C in Figure 4c). In addition, substantial erosion occurs related to channel incision and the formation of new channels via avulsion (e.g., Area D in Figure 4c). It is also possible to make inferences about the actual process of sediment transport. For example, although there are several channels in the braided river, sediment movement may be limited to only certain channels and parts of those channels, and may not occur at all in others (some channels are present in both DEMs, but absent from the DEM of difference). Thus, rather than a continuous conveyer belt for sediment transport, the process of sediment transfer is variable, and occasionally discontinuous, in time and space. Sediment moves in stages from discrete erosion sites to discrete deposition sites, within the flume, and areas of extensive erosion are often succeeded a short distance downstream by deposition. This is apparent in the length of channel between points A and B in Figure 4c. Here, erosional widening and migration of the channel apparently provided the upstream sediment supply to the bar deposited in the next bend downstream. This type of spatial arrangement also provides evidence for the typical transfer distance from erosion site to associated deposition site.

Measurement of Erosion/Deposition Volumes for Estimation of Sediment Transport Rate

Quantification of morphological change has an important application as a method for measuring average sediment transport rate in the reach, as well as the spatial and temporal patterns of transport (Ashmore and Church, in press). With rates of input and/or output of sediment to the reach (flume) known, the volumes and time interval of change, and the net difference between erosion and deposition, are all that are required to calculate the sediment budget for the reach. From this, the reach-averaged transport rate and the rate of change of transport in the downstream direction can be estimated (Lane *et al.*, 1995).

In the experiment described here, the difference between input and output of sediment during any time step serves as an independent check on the accuracy of the volumes measured by differencing of DEMs for the entire model. Alternatively, the model can be divided into a series of "slices," and the budget can be propagated downstream from slice to slice,

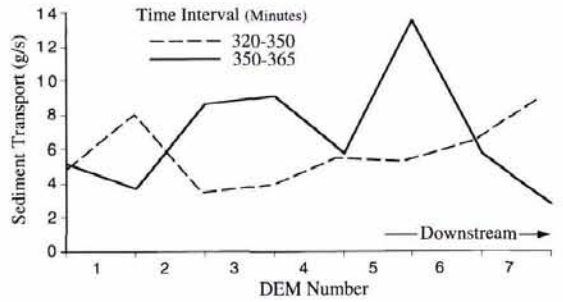

Figure 5. Downstream variation in bed material transport rate between the 350 and 320 time epochs, and 365 and 320 time epochs. At constant water discharge, sediment transport rate varies spatially at one epoch, and temporally between epochs.

beginning with the measured input at the upstream end. Figure 5 shows the downstream variation in total sediment transport rate through seven separate slices of the model at two time periods. In practice, this could be done for many more slices, and also for the cross-channel variation. Although water discharge is identical for the two cases, both mean transport and the downstream variation in transport rate differ between the two cases. For example, the reach encompassing frame numbers 4-8 shows net erosion throughout (transport rate increases steadily in the downstream direction) in the 350-320 epoch (Figure 5). But the same reach has a more complex pattern, with much of it showing net deposition in the 365-350 epoch.

The output measured from volumetric change can be compared with the actual output recorded at the time of the experiment. If these results show that the volumes of change measured from the DEMs are accurate, the results can then be used to assess the effect of certain assumptions and errors which are inherent in the application of the "inverse" method for estimating bedload transport rate (Ashmore and Church, in press). These include the estimation of the typical transfer distance for sediment (downstream spacing of discrete erosion and deposition sites), the magnitude of the underestimation of transport rate due to unknown input and/or output to the reach, the underestimation due to compensating scour and fill at a point, and the effect of spatial interpolation from sparse survey data on the accuracy and precision of volume estimates.

At present, results are promising but variable. In some cases, the results are equivalent to the recorded volume change; in others, the outcome is less convincing. Figure 6 shows a scatterplot depicting correlations between the estimated and recorded volumes for 20 DEMs of difference.

In an attempt to determine the precision of the estimated volume differences, a full propagation of variance was performed by assuming that the elevation of each pixel used in the volume calculation was ± 1.7 mm. This error propagation suggested that the estimated volumetric change should indeed be very precise. The differences between the estimated and recorded volumes is clearly larger than such a confidence region (even at the 99 percent level of significance), suggesting that the derived DEMs are comparatively inaccurate, possibly due to some deficiency in the photogrammetric functional models. However, the propagation of variance process assumes that the volume derived using the elevation of each pixel estimate is independent of any neighboring values, yet the nature of the sediment budget used to estimate volumes of change assumes direct correlation. Clearly, any minor error in the functional model will affect all pixels within a region, and small changes over large areas will create noticeable changes in volume differencing. Such correlation suggests that simple variance propagation provides far too optimistic an estimate of the precision of derived volume differences and that it is inadequate for examining the stochastic aspects of this type of problem.

Discussion

One of the important reasons for carrying out the experimental work was to assess the potential of estimating river bed material transport rates by measurement of morphological change (Ashmore and Church, 1995). Automated DEM acquisition methods were very successful in generating the data necessary to represent the flume at a sufficiently high resolution at all 19 epochs. Manual data acquisition methods based upon analytical photogrammetry cannot practically provide DEMs of the required resolution. Despite the success of generating these data sets, there is some inconsistency between the morphological change determined by digital photogrammetry and by direct measurement. It was, therefore, essential to consider further the quality of the derived DEMs and to examine potential systematic error sources.

Quality of the Automatically Derived DEMs

The quality of each automatically derived DEM was assessed in terms of the precision and accuracy of the measured surfaces. The average minimum and maximum precision for generated points determined by the OrthoMAX algorithm was approximately 0.50 and 0.05 pixels (6.3 and 0.6 μm), respectively. By incorporating photo-coordinate measurements with these stochastical properties in a bundle adjustment, it was possible to determine the expected precision of determined object coordinates. This suggested that the precision of the

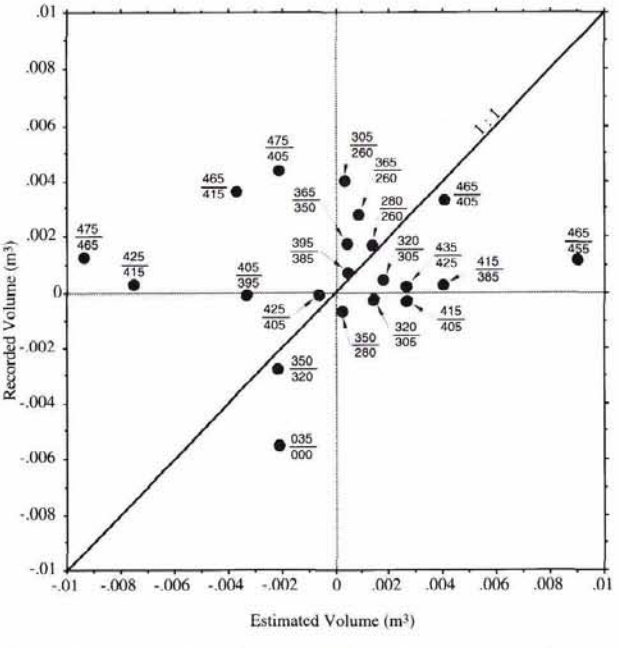

Figure 6. Scatterplot of the recorded changes in volume (measured sediment input and output in each epoch) versus the estimated changes in volume (calculated from volumes of change in successive DEMs). The numbers (e.g., 320/305) adjacent to each point refer to the time period used for the calculation.

elevation of object coordinates would be expected to be between ±1.7 and ±0.5 mm and broadly agrees with the accuracy assessments carried out for the bundle adjustments using GAP and OrthoMAX.

In order to assess the accuracy of the automatic DEM collection technique, other tests were carried out. The overlapping areas of two adjacent DEMs extracted at epoch 260 minutes were subtracted from one another. Figure 7 illustrates DEM 1 generated using negatives 45 and 46, DEM 2 generated using negatives 46 and 47, and the difference in elevation between the overlapping areas of the two DEMs. The mean and standard deviation values for the overlapping areas depicting differences in elevation are 0.7 mm and 0.6 mm, respectively. Errors of 15 mm and greater exist along the left and right boundaries of the overlapping areas. Of interest are the two curves representing steps in elevation which are apparent on the left and right limits of each DEM (i.e., the Figure 7 curve located on the left boundary of DEM 2). The probability of error associated with the estimation of a point increases with distance away from the center of a DEM. For example, the variation in elevation along line a to b, shown on DEM 2 (Figure 7), is 0.012 m. Such a systematic trend in the data suggests the presence of systematic error and was noticed during initial data extraction. It was decided to minimize the impact of such an error by extracting only the sub-scene portions of each DEM. The systematic error evident in Figure 7 was thought to be attributable to uncertainties associated with the unknown inner geometry of the non-metric camera, and tests were carried out in order to isolate the cause.

The Search for Possible Systematic Error Sources

The lens model which was used for the final data extraction was determined using self-calibration methods by incorporating manually measured photo coordinates using only six oblique photographs. It seemed prudent to assess the impact of a revised camera model derived by combining measurements from the oblique imagery with those from one of the strips of vertical photographs used for data extraction. A comparison between the two camera models derived from the two sets of photo coordinates is given in Table 2. Two

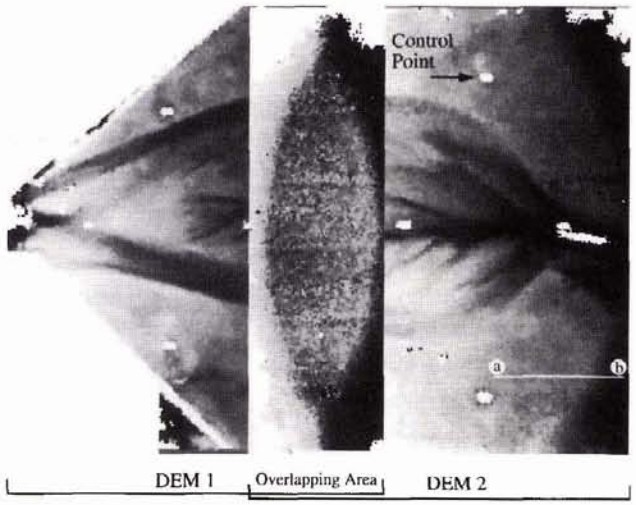

Figure 7. Systematic errors apparent in overlapping areas of independent DEMs. The central portion of the figure shows differences between elevations in common areas on the two DEMs. At the corners of the overlapping areas, discrepancies are up to 15 mm.

TABLE 2. COMPARISON OF TWO CAMERA MODELS DERIVED USING OBLIQUE PHOTOGRAPHS AND COMBINED OBLIQUE AND VERTICAL PHOTOGRAPHS

Interior Orientation Parameters	Six Oblique Images	Six Oblique and Eight Vertical Images
Focal Length (mm)	58.9237 (±0.093)	58.1803 (±0.034)
x_p (mm)	0.1808 (±0.041)	0.2777 (±0.035)
y_p (mm)	−0.2076 (±0.046)	−0.2200 (±0.043)
K_1 (m^{-2})	−21.604 (±1.21)	−22.265 (±0.496)
K_2 (m^{-4})	3958.2 (±1620)	5440.8 (±476)

DEMs were generated over the same area but with the differing camera models and then were subtracted from one another. This DEM of difference was then used to generate a histogram of differences, illustrated by Figure 8.

What is immediately apparent from the distribution is a shift of the mean value to approximately 0.9 mm below zero, suggesting that the missing systematic error source has been identified. It has to be remembered that the same calibration data would have been enforced for all images at all epochs, and so all data contained in the derived DEM would be offset by the same small amount. The distribution is normal, although exhibiting some degree of kurtosis, and examination of the distribution of DEM differences in the image reveals no variation in the size of the differences towards the edge of the format. It can be concluded that this is not the missing error source.

A further area of concern experienced when restituting nonmetric imagery is the lack of calibrated fiducial marks and consequent uncertainty of establishing accurate interior-orientation parameters during fiducial/reference mark measurement. To assess the impact of introducing such a systematic error into the restitution process, two DEMs were generated of the same area using a model derived using an acceptable affine transformation (±5-μm residuals) and one which was deliberately downgraded (±50-μm residuals). A DEM of difference was generated and a histogram was produced (Figure 9).

The histogram is normally distributed about a mean of zero, exhibiting a standard deviation of ± 1 mm. The absence of a shift in average elevation is surprising, but is consistent with earlier derived DEMs. It can be concluded,

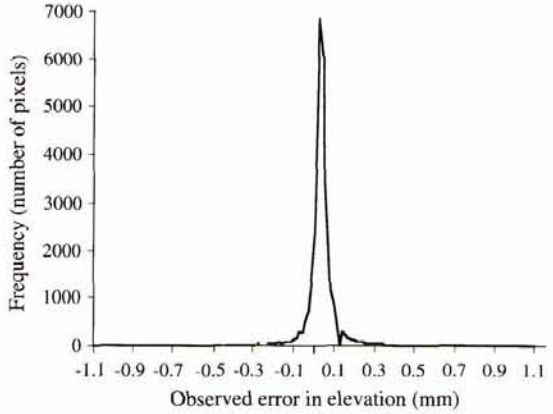

Figure 8. Histogram of differences between a DEM calculated from a camera model derived from obliques and a DEM calculated from a model derived from obliques and verticals. No systematic effect of camera model is detected in the results.

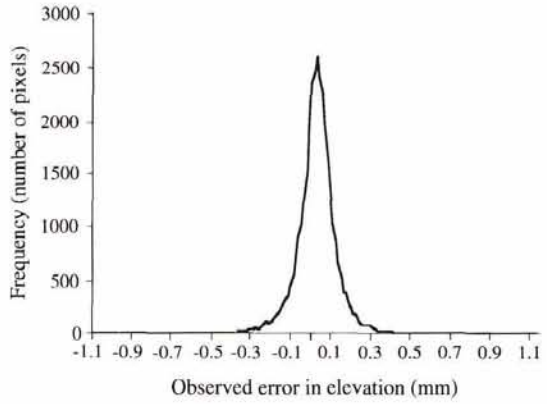

Figure 9. Histogram of differences between two DEMs calculated from good and poor affine transformation parameters to test the effect of errors due to lack of precision in identifying corners of format. Lack of good fiducial data is not responsible for DEM error.

therefore, that the uncertainties emanating from the lack of fiducial data are insufficient to distort the derived DEMs significantly. The remaining minor systematic error source remains elusive.

Conclusions

The presented research was successful in deriving dense elevation models of a physical scale model of a braided river using automated DEM extraction techniques from non-metric photography. Using a self calibrating bundle adjustment, the calibration parameters associated with the non-metric photography were successfully estimated to approximately ± 0.05 mm and derived control-point coordinate RMS errors were approximately ±0.0015 m. Using ERDAS OrthoMAX for photogrammetric restitution, results obtained from the triangulation performed on the eight photographs comprising a strip suggested a precision of approximately 1.8 mm. The eight exposure-station coordinates were estimated to a precision of approximately ±1.5 mm. The precision of the automated DEM extraction technique were on the order of ± 0.05 pixel, indicating success in matching corresponding points on several images. The precision of the automatically generated DEMs was calculated to be within the range of ±0.5 mm to ±1.7mm. The DEMs of difference provide valuable geomorphic data which give an insight into the spatial patterns of erosion and deposition through time. The idea of using estimated volumes of erosion and deposition to estimate sediment transport rates has been hindered by minor, although significant, errors in the DEM data. It is suspected that such inaccuracies are attributable to over-simplification of the functional models used to recover the geometry of the inner cone of the non-metric camera. Remaining systematic errors may be attributed to film deformation, uncompensated residual lens distortion, or small distortions created by the adapted method of interior orientation and will be difficult to resolve. However, future research will include further analysis and minimization of those systematic errors in the DEMs and resolution of datum errors that exist between independent DEMs.

Acknowledgments

This research is supported by a Research Grant to P. Ashmore from the Natural Sciences and Engineering Research Council, Canada. Additional support for the experimental work was provided by the Canterbury Regional Council, New Zealand. The experiments were carried out in the Hydraulics Laboratory, Department of Natural Resources Engineering, Lincoln University, New Zealand while P. Ashmore was Visiting Lecturer in the Department of Geography, University of Canterbury. We are grateful to those institutions for their support and particularly to Tim Davies for access to his "braided river flume." P. Ashmore's discussions with, and advice from, Tim Davies, George Griffiths, and Alex Sutherland were a great help in the early stages of the research. We also thank the Photogrammetry Research Unit (Roger Littleworth and Stuart Robson), City University, London for assistance with image scanning.

References

Albertz, J., and J. Kreiling, 1989. *Photogrammetric Guide*, Herbert Wichmann Verlag, Karsruhe, 284 p.

Ashmore, P.E., and M. Church, in press. Sediment transport and river morphology: a paradigm for study, *Gravel-bed Rivers in the Environment, Proceedings of Gravel-bed Rivers IV International Workshop*, Gold Bar, Washington, 1995.

Brunsden, D., and J.H. Chandler, 1996. The continuing evolution of the Black Ven mudslide, 1946-95, *Advances in Hillslope Processes* (S. Brooks and M. Anderson, editors), Wiley, Chichester, pp. 869–898.

Chandler, J.H., J.S. Clark, M.A.R. Cooper, and D.M. Stirling, 1987. Analytical photogrammetry applied to Nepalese slope morphology, *Photogrammetric Record*, 12(70):443–458.

Chandler, J.H., and R. Moore, 1989. Analytical photogrammetry: A method for monitoring slope instability, *Quarterly Journal of Engineering Geology*, 22:97–110.

Chandler, J.H., M.A.R. Cooper, and S. Robson, 1989. Analytical aspects of small format surveys using oblique aerial photography, *The Journal of Photographic Science*, 37:235–240.

Chandler, J.H., and D. Brunsden, 1995. Steady state behaviour of the Black Ven mudslide: The application of archival analytical photogrammetry to studies of landform change, *Earth Surface Processes and Landforms*, 20:255–275.

Collin, R.L., and N.W.T. Chisholm, 1991. Geomorphological photogrammetry, *Photogrammetric Record*, 13(78):845–854.

Collins, S.H., and G.C. Moon, 1979. Stereometric measurement of streambank erosion, *Photogrammetric Engineering & Remote Sensing*, 45:183–190.

Cooper, M.A.R., 1987. *Control Surveys in Civil Engineering*, Nichols Publishing Company, New York, 381 p.

Dixon, L.F.J., R. Barker, M. Bray, P. Farres, J. Hooke, R. Inkpen, A. Merel, D. Payne, and A. Shelford, 1996. Analytical photogrammetry for geomorphological research, *Landform Measurement, Modelling and analysis* (S.N. Lane, K.S. Richards, and J.H. Chandler, editors), in press.

ERDAS, 1995. *Imagine OrthoMAX Users Guide, Version 8.2*, Vision International & ERDAS, Inc., Atlanta, Georgia.

Fraser, C.S., 1989. Photogrammetric monitoring of Turtle Mountain: A feasibility study, *Photogrammetric Engineering & Remote Sensing*, 49:1551–1559.

Fryer, J.G., J.H. Chandler, and M.A.R. Cooper, 1994. On the accuracy of heighting from maps and aerial photographs: Implications for process modellers, *Earth Surface Processes and Landforms*, 19: 577–583.

Granshaw, S.I., 1980. Bundle adjustment methods in engineering photogrammetry, *Photogrammetric Record*, 10(56):181–207.

Jäggi, M., 1975. *Anwendung der Photogrammetrie bei hydraulischen Modellversuchen*, Miitteilung der Versuchsanstalt für Wasserbau, Hydrologie und Glaziologie, No. 16, Der Eidgenössischen Technischen Hochschule Zürich, 95 p.

Kenefick, J.F., M.S. Gyer, and B.F. Harp, 1972. Analytical self-calibration, *Photogrammetric Engineering & Remote Sensing*, 38: 1117–1126.

Lane, S., K.S. Richards, and J.H. Chandler, 1993. Developments in photogrammetry; the geomorphological potential, *Progress in Physical Geography*, 17(3):306–328.

———, 1994. Applications of distributed sensitivity analysis to a model of turbulent open channel flow in a natural river channel, *Proceedings of the Royal Society*, Series A, pp. 49–63.

———, 1995. Morphological estimation of the time-integrated bed load transport rate, *Water Resources Research*, 31:761–772.

Lewin, J., and M.J.C. Weir, 1977. Morphology and recent history of the Lower Spey, *Scottish Geographical Magazine*, 93:43–51.

Murray, A.B., and C. Paola, 1994. A cellular model of braided rivers, *Nature*, 371:54–57.

———, 1996. A new quantitative test of geomorphic models, applied to a model of braided streams, *Water Resources Research*, 32: 2579–2587.

Nolette, C., P.A. Gagnon, and J.P. Agnard, 1992. The DVP: Design, operation, and performance, *Photogrammetric Engineering & Remote Sensing*, 58:65–69.

Patias, P., and A. Streilein, 1996. Contribution of videogrammetry to the architectural restitution - Results of the CIPA "O.Wagner Pavillion" Test, *International Archive of Photogrammetry and Remote Sensing*, 31(Part B5):457–462.

Smith, M., 1987. *Photogrammetric Techniques for Archaeological Mapping Using Oblique Non-Metric Photography*, unpublished PhD thesis, University College London, 230 p.

Welch, R., and T.R. Jordan, 1983. Analytical non-metric close-range photogrammetry for monitoring stream channel erosion, *Photogrammetric Engineering & Remote Sensing*, 49(3):367–374.

(Received 15 November 1996; revised and accepted 07 November 1997)

Forthcoming Articles

John E. Anderson, **Spectral Reflectance and Detection of Iron-Oxide Precipitates Associated with Acidic Mine Drainage.**

Michel Arnaud and *Albert Flori*, **Bias and Precision of Different Sampling Methods for GPS Positions.**

Edward A. Ashton and *Alan Schaum*, **Algorithms for the Detection of Sub-Pixel Targets in Multispectral Imagery.**

Mark J. Carlotto, **Spectral Shape Classification of Landsat Thematic Mapper Imagery.**

Stéphane Chalifoux, François Cavayas, and *James T. Gray*, **Map-Guided Approach for the Automatic Detection on Landsat TM Images of Forest Stands Damaged by the Spruce Budworm.**

F.M. Danson, **Teaching the Physical Principles of Vegetation Canopy Reflectance Using the SAIL Model.**

George F. Hepner, Bijan Houshmand, Igor Kulikov, and *Nevin Bryant*, **Investigation of the Integration of AVIRIS and IFSAR for Urban Analysis.**

Michael E. Hodgson, **What Size Window for Image Classification? — A Cognitive Perspective.**

Taejung Kim and *Jan-Peter Muller*, **A Technique for 3D Building Reconstruction.**

Magaly Koch and *Farouk El-Baz*, **Identifying the Effects of the Gulf War on the Geomorphic Features of Kuwait by Remote Sensing and GIS.**

Rongxing Li, **Potential of High-Resolution Satellite Imagery for National Mapping Products.**

Ross S. Lunetta, John G. Lyon, Bert Guindon, and *Christopher D. Elvidge*, **North American Landscape Characterization Dataset Development and Data Fusion Issues.**

Kenneth C. McGwire, **Mosaicking Airborne Scanner Data with the Multiquadric Rectification Technique.**

Kenneth C. McGwire, **Improving Landsat Scene Selection Systems.**

John G. Mickelson, Jr., Daniel L. Civco, and *John A. Silander, Jr.*, **Delineating Forest Canopy Species in the Northeastern United States Using Multi-Temporal TM Imagery.**

S.V. Muller, D.A. Walker, F.E. Nelson, N.A. Auerbach, J.G. Bockheim, S. Guyer, and *D. Sherba*, **Accuracy Assessment of a Land-Cover Map of the Kuparuk River Basin Alaska: Considerations for Remote Regions.**

Elijah W. Ramsey III, Dal K. Chappell, Dennis Jacobs, Sijan K. Sapkota, and *Dan G. Baldwin*, **Resource Management of Forested Wetlands: Hurricane Impact and Recovery Mapped by Combining Landsat TM and NOAA AVHRR Data.**

E. Terrence Slonecker, Denice M. Shaw, and *Thomas M. Lillesand*, **Emerging Legal and Ethical Issues in Advanced Remote Sensing Technology.**

David M. Stoms, Michael J. Bueno, Frank W. Davis, Kelly M. Cassidy, Kenneth L. Driese, and *James S. Kagan*, **Map-Guided Classification of Regional Land-Cover with Multi-Temporal AVHRR Data.**

Chuang Tao, Rongxing Li, and *Michael A. Chapman*, **Automatic Reconstruction of Road Centerlines from Mobile Mapping Image Sequences.**

Stella W. Todd and *Roger M. Hoffer*, **Responses of Spectral Indices to Variations in Vegetation Cover and Soil Background.**

Randolph H. Wynne, Thomas M. Lillesand, Murray K. Clayton, and *John J. Magnuson*, **Satellite Monitoring of Lake Ice Breakup on the Laurentian Shield (1980-1994).**